Ferromagnetism in nanoscale BiFeO$_3$

R. Mazumder, P. Sujatha Devi, Dipten Bhattacharya,[a] P. Choudhury, and A. Sen
Sensor and Actuator Section, Central Glass and Ceramic Research Institute, Kolkata 700032, India

M. Raja
Defense Metallurgical Research Laboratory, Hyderabad 500058, India

A remarkably high saturation magnetization of $\sim 0.4 \mu_B$/Fe along with room temperature ferromagnetic hysteresis loop has been observed in nanoscale (4–40 nm) multiferroic BiFeO$_3$ which in bulk form exhibits weak magnetization ($\sim 0.02 \mu_B$/Fe) and an antiferromagnetic order. The magnetic hysteresis loops exhibit exchange bias and vertical asymmetry which could be because of spin pinning at the boundaries between ferromagnetic and antiferromagnetic domains. Interestingly, both the calorimetric and dielectric permittivity data in nanoscale BiFeO$_3$ exhibit characteristic features at the magnetic transition point. These features establish the formation of a true ferromagnetic-ferroelectric system with a coupling between the respective order parameters in nanoscale BiFeO$_3$. © *2007 American Institute of Physics*. [DOI: 10.1063/1.2768201]

During the last few years, there has been a resurgence in research in the area of multiferroics with identification of three different genres of multiferroic systems: (i) systems where magnetism and ferroelectricity originate in different sublattices[1]—e.g., in BiFeO$_3$—where Bi–O orbital hybridization (or covalency) due to Bi $6s^2$ lone pair is responsible for the ferroelectric instability while Fe–O–Fe antisymmetric Dzyaloshinskii-Moriya exchange gives rise to a complicated magnetic order; (ii) systems where incommensurate spiral magnetic structure breaks down the spatial inversion symmetry[2] and thereby gives rise to ferroelectricity—e.g., in TbMnO$_3$; and (iii) systems where elastic interaction at the interface of ferroelectric-magnetic superlattice structure governs the multiferroicity—e.g., in BaTiO$_3$–CoFe$_2$O$_4$ multilayers.[3] Yet none of these systems exhibit strong coupling between electrical polarization (**P**) and magnetization (**M**) near room temperature which is important for practical applications. In this backdrop, the improvement in the magnetization of BiFeO$_3$ assumes importance because such improvement can help in utilizing the room temperature multiferroicity of BiFeO$_3$ ($T_C \sim 1103$ K and $T_N \sim 643$ K) for practical applications. In spite of room temperature multiferroicity, bulk BiFeO$_3$ suffers from poor magnetization (0.02μ_B/Fe) and inhomogeneity which gives rise to leakage. We report here that a remarkably high saturation magnetization ($M_s \sim 0.4 \mu_B$/Fe) could be observed in nanoscale BiFeO$_3$ prepared by a solution chemistry route. Interestingly, even this ferromagnetic BiFeO$_3$ exhibits characteristic features in calorimetric and dielectric properties around the magnetic transition temperature (T^*), highlighting useful multiferroic behavior. It has already been recognized that suppression of helical order—which exists with a periodicity ~ 620 Å on canted antiferromagnetic order between two successive (111) ferromagnetic planes[4]—might give rise to higher magnetization. The decrease in particle size below the periodicity of the helical order can give rise to suppression of the helical order.[5]

The nanosized powders of BiFeO$_3$ have been prepared by the glycine combustion synthesis process.[6] A mixture of aqueous solutions of bismuth nitrate and ferric nitrate is used as oxidant and glycine is added as a fuel. A glycine to nitrate ratio of 0.1 has resulted in the formation of nearly phase pure nanoparticles of BiFeO$_3$. The as-prepared powder is calcined at different temperatures within 300–700 °C for 4–6 h in order to vary the particle size over 4–40 nm. The x-ray diffraction (XRD) patterns for all the cases have been studied at room temperature. The particle morphology and the local crystallographic structure have been studied by transmission electron microscopy (TEM), selected area electron diffraction (SAED), and high resolution transmission electron microscopy (HRTEM), respectively. The magnetic hysteresis loops over a field range $\sim \pm 1.5$ T have been measured at room temperature for all these powders. The calorimetric and dielectric properties have also been measured across the magnetic transition point (T^*). The heat-treatment temperature and time, particle size, and saturation magnetization values corresponding to different samples (S1, S2, S3, and S4) are given in Table I.

The XRD pattern for nanoscale BiFeO$_3$ (S3) is shown in Fig. 1. The data are taken with step size of 0.017° (2θ) and step time of 25 s by using an advanced system of accelerator detector array. Such a detector system improves the resolution beyond what is normally achieved. The patterns collected thus for both the bulk and nanoscale BiFeO$_3$ have been refined by FULLPROF (ver 2.3, 2003) using space group $R3c$. The lattice parameters, structure parameters, such as bond angle, bond length, etc., as well as the microstrain in the particles have been estimated and are shown in Table II. It is quite clear that the lattice strain in nanoscale particles is nearly twice as large. Minor impurities such as Bi$_2$Fe$_4$O$_9$ (file: 20-0836) and Bi$_{24}$Fe$_2$O$_{39}$ (file: 42-0201) are found to be present in nanoscale system. The quantitative estimation

TABLE I. Relevant parameters of the nanoscale BiFeO$_3$ samples.

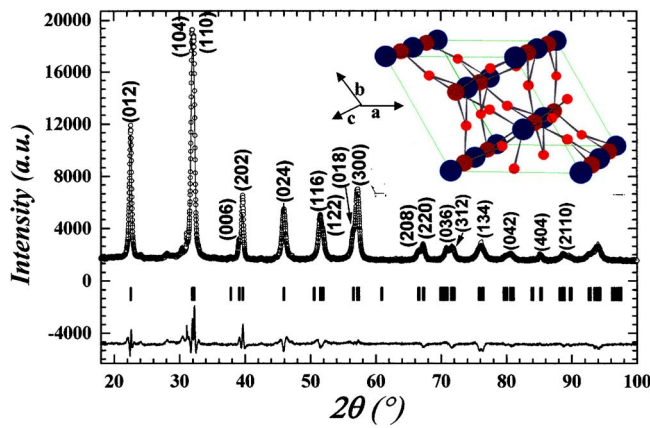| Sample name	Heat-treatment schedule	Particle size (nm)	M_s (μ_B/Fe)
S1	Untreated	4	0.41
S2	300 °C/6 h	15	0.27
S3	450 °C/6 h	25	0.13
S4	450 °C/48 h	40	0.09

[a]Electronic mail: dipten@cgcri.res.in

FIG. 1. (Color online) X-ray diffraction patterns for nanoscale BiFeO$_3$ (S3) refined by FULLPROF (ver 2.3, 2003). The insets show that the cells with big, medium, and small spheres correspond to Bi, Fe, and O, respectively.
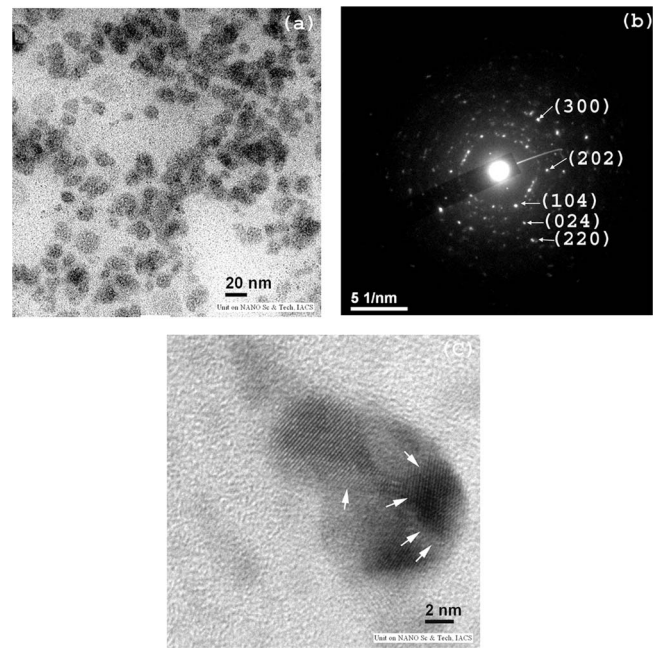

FIG. 2. (a) TEM, (b) SAED pattern, and (c) HRTEM photographs of nanoscale BiFeO$_3$ (S3); the interfaces are shown in the HRTEM photograph by arrows.

shows the total concentration of impurities to be <3%. However, none of these impurities are ferromagnetic at room temperature.[7] Therefore, the room temperature ferromagnetic property observed here cannot result from any one of them. It has been pointed out earlier[8] that the presence of ferrimagnetic ($T_C \sim 850$ K) cubic γ-Fe$_2$O$_3$ impurity is responsible for higher saturation magnetization in many cases. In our case, of course, such a phase is clearly absent.

In Fig. 2, we show the representative TEM, SAED, and HRTEM photographs of the BiFeO$_3$ nanoparticles (S3). Both the SAED and HRTEM results are pointing out that the particles are essentially multidomain with the presence of interfaces between two phases—ferromagnetic (oxygen deficient) and antiferromagnetic (stoichiometric) BiFeO$_3$. Using thermogravimetry data, the oxygen deficiency δ is calculated to be $\sim$0.05 in BiFeO$_{3-\delta}$. The deterioration of the room temperature ferromagnetism, observed in samples annealed under oxygen at 450 °C for 6 h, shows that the oxygen deficiency has a role to play for ferromagnetism. The diffraction spots in the SAED pattern could be indexed as the (104), (220), (202), and (024) planes of BiFeO$_3$. The lattice fringes in HRTEM photographs are identified to be the (104), (202), (012), and (024) planes of BiFeO$_3$ phase across all the domains. No trace of γ-Fe$_2$O$_3$ phase could be observed in both these data.

The magnetic hysteresis loops have been measured over $\pm$1.5 T at room temperature (Fig. 3). All the loops exhibit finite exchange bias field and vertical asymmetry (ΔM). The right *y* scale of Fig. 3 depicts the magnetization of the bulk

BiFeO$_3$ under identical condition. With the increase in particle size, the saturation magnetization (M_s) decreases (inset of Fig. 3). Both the M_s and the ΔM scale are nearly identical patterns with particle size (d). It appears, therefore, that the interface area also decreases with the increase in particle size. The exchange bias field H_{eb} [=$(H_{c1}-H_{c2})/2$; H_{c1} and H_{c2} are the negative and positive coercive fields, respectively] varies within 110–275 Oe (error bar $\sim \pm 5$%) for particles of different sizes. Finite coercivity and H_{eb} even at room temperature rule out the possibility of superparamagnetism in nanoscale BiFeO$_3$. Instead, it confirms the ferromagnetic order as well as spin pinning at the ferromagnetic-antiferromagnetic interfaces.[9]

In Fig. 4, we show the calorimetric trace along with the representative dielectric permittivity versus temperature plot across the magnetic transition point T^* for sample S4. The dielectric property has been measured by compacting the nanoscale powder and heat treating the samples under a moderately high temperature ($\sim$450 °C). The anomaly at the magnetic transition point T^* is conspicuous in both these plots. It is to be noted that T^* is $\sim$633 K in the nanoscale

TABLE II. Relevant parameters from Rietveld refinement XRD pattern of bulk and nanoscale BiFeO$_3$ (S3); space group $R3c$.

| Lattice parameters			Atom coordinates			R_p	R_{wp}	χ^2		Bond length	Bond angle	Microstrain (%)
			x	y	z							
						BiFeO$_3$ (bulk)						
a=5.578 Å	Bi	6a	0	0	0				Bi–O	2.309 Å	Fe–O–Fe 154.05°	0.015
c=13.868 Å	Fe	6a	0	0	0.2198	13.6	22.6	2.17	Fe–O	1.949 Å	O–Bi–O 73.88°	
	O	18b	0.4346	0.0121	−0.0468				Fe–O	2.118 Å		
						BiFeO$_3$ (nanoscale)						
a=5.573 Å	Bi	6a	0	0	0				Bi–O	2.13 Å	Fe–O–Fe 152.76°	0.029
c=13.849 Å	Fe	6a	0	0	0.22324	4.91	6.68	9.51	Fe–O	1.804 Å	O–Bi–O 78.93°	
	O	18b	0.4715	0.0119	−0.0622				Fe–O	2.269 Å		
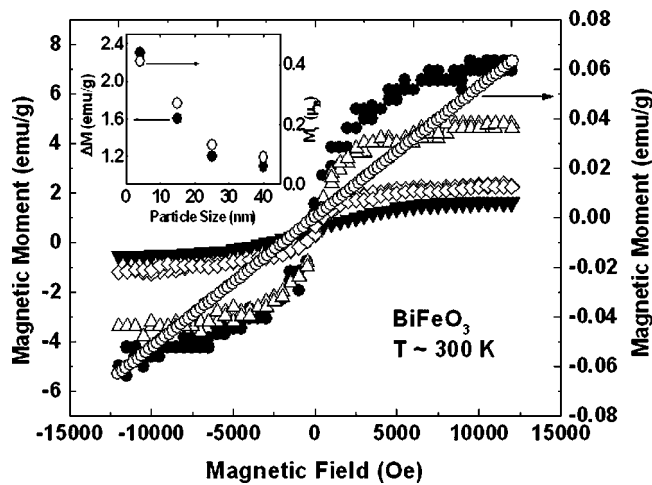
FIG. 3. Magnetic hysteresis loops for nanoscale (4–40 nm) and bulk samples (open circle). Inset: the M_s (open circle) and ΔM (solid circle) vs particle size (d) patterns are shown.

BiFeO$_3$ sample. In contrast, T_N is ~643 K for the bulk BiFeO$_3$. The peak in the calorimetric trace around the magnetic transition point T^* signifies that the transition is first order in nature.[10] This is possible due to coexistence of paramagnetic and antiferromagnetic phases near the boundary following Landau-Devonshire theory of phase transition. It has been shown by a recent theoretical model calculation that the strong coupling between the lattice strain and electronic structure (such as orbital order) gives rise to first order transition.[11] Weak coupling, on the other hand, gives rise to higher order transition. Higher lattice strain (Table II) in nanoscale BiFeO$_3$, possibly, induces stronger coupling. The dielectric anomaly (main frame of Fig. 4) around T^* signifies coupling between polarization (**P**) and magnetization (**M**), as expected in any multiferroic system such as BiFeO$_3$. Both the real and imaginary parts (ε' and ε'') of the dielectric permittivity exhibit anomaly around T^*. Of course, there is a slight mismatch between T^* identified in calorimetric (~633 K) and dielectric data (~624 K). Moreover, a transition zone ($\Delta T^* = T^* - T^*_{\text{onset}} = 80$ K) is apparent in the dielectric data. This could be because of a broader transition process expected in the nanoscale system. The ε'' is also quite high due to the high conductivity of the samples, especially at higher temperature. However, the anomaly in the dielectric

permittivity shows that the ferromagnetic phase of BiFeO$_3$ is coupled to the electric polarization which is essential for a true multiferroic system. The *observations* of room temperature ferromagnetism and the *coupling* between ferromagnetic and ferroelectric order parameters are the central results of this letter.

There could be a combination of three factors behind the improvement in the magnetization in nanoscale particles: (i) suppression of helical order, i.e., incomplete rotation of the spins along the direction of the wave vector, (ii) increase in spin canting, due to the lattice strain which gives rise to weak ferromagnetism, and (iii) oxygen deficiency. The enhanced canting angle is found to have given rise to higher M_s in epitaxial thin films.[12] Incidentally, in our case too, we observe the increase in lattice strain in finer particles. Moreover, the oxygen deficiency also plays a minor role here as it forms Fe^{2+} (with magnetic moment ~6.7μ_B against ~5.92μ_B in Fe^{3+}) and, possibly, gives rise to carrier-mediated local ferromagnetic order across Fe^{3+}–O^{2-}–Fe^{2+} (Ref. 13). It is worthwhile to recall here that the M_s is nearly four times higher (~0.4μ_B/Fe) in the samples prepared by us compared to what is reported very recently (~0.11μ_B/Fe) in strain-free particles.[5] It appears that both the suppression of helical order as well as enhanced canting together with oxygen deficiency give rise to even higher M_s in our case.

In summary, we show here that nanoscale BiFeO$_3$ depicts quite high saturation magnetization as well as genuine ferromagnetic behavior with finite coercivity at room temperature. Interestingly, such a system retains the coupling between magnetization and electrical polarization and hence could prove to be quite useful for developing nanoscale multiferroic devices based on BiFeO$_3$.
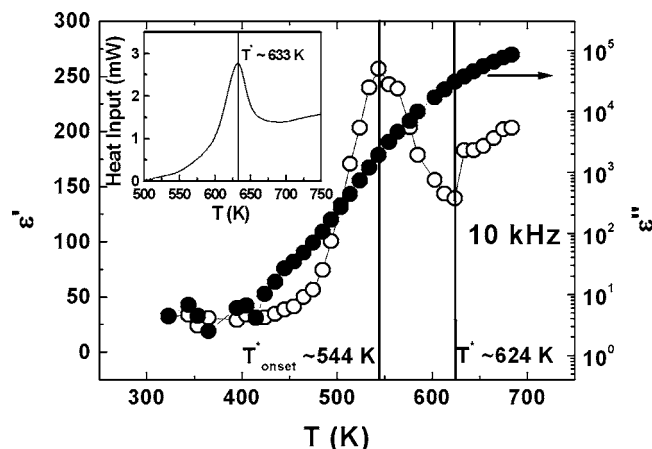
FIG. 4. Real and imaginary parts of the dielectric permittivity [$\varepsilon'(\omega,T)$, $\varepsilon''(\omega,T)$] vs temperature plot across the magnetic transition points T^*_{onset} and T^* for nanoscale BiFeO$_3$ (S4). The inset shows the corresponding differential scanning calorimetry thermogram.

[1] See, for example, H. Schmidt, Ferroelectrics **162**, 317 (1994).
[2] See, for example, S.-W. Cheong and M. Mostovoy, Nat. Mater. **6**, 13 (2007).
[3] See, for example, R. Ramesh and N. A. Spaldin, Nat. Mater. **6**, 21 (2007).
[4] I. Sosnowska, T. Paterlin-Neumaier, and E. Steichele, J. Phys. C **15**, 4835 (1982).
[5] T.-J. Park, G. C. Papaefthymiou, A. J. Viescas, A. R. Moodenbough, and S. S. Wong, Nano Lett. **7**, 766 (2007).
[6] S. Banerjee and P. S. Devi, J. Nanopart. Res. (in press).
[7] N. Shamir, E. Gurewitz, and H. Shaked, Acta Crystallogr., Sect. A: Cryst. Phys., Diffr., Theor. Gen. Crystallogr. **A34**, 662 (1978).
[8] H. Bea, M. Bibes, S. Fusil, K. Bouzehouane, E. Jacquet, K. Rode, P. Bencock, and A. Barthèlémy, Phys. Rev. B **74**, 020101(R) (2006).
[9] See, for example, J. Nogues and I. K. Schuller, J. Magn. Magn. Mater. **192**, 203 (1999); See also, A. Mumtaz, K. Maaz, B. Janjua, and S. K. Hasanain, e-print arXiv:nlin/060427.
[10] V. R. Palkar, J. John, and R. Pinto, Appl. Phys. Lett. **80**, 1628 (2002).
[11] T. Maitra, P. Thalmeier, and T. Chatterji, Phys. Rev. B **69**, 132417 (2004).
[12] J. Wang, J. B. Neaton, H. Zheng, V. Nagarajan, S. B. Ogale, B. Liu, D. Viehland, V. Vaithyanathan, D. G. Scholm, U. V. Waghmare, N. A. Spaldin, K. M. Rabe, M. Wuttig, and R. Ramesh, Science **299**, 1719 (2003).
[13] See, for example, M. J. Calderón and S. Das Sarma, e-print arXiv:cond-mat/0603182; D. H. Ridgley, H. Lessoff, and J. D. Childress, J. Am. Ceram. Soc. **53**, 304 (1970); X. H. Zhou, X. S. Chen, Y. Huang, H. Duan, and W. Lu, Phys. Status Solidi B **243**, 1375 (2006).